

# Chiral particle separation by a non-chiral micro-lattice

Lukas Bogunovic<sup>1</sup>, Marc Fliedner<sup>1</sup>, Ralf Eichhorn<sup>2</sup>, Sonja Wegener<sup>1</sup>, Jan Regtmeier<sup>1</sup>, Dario Anselmetti<sup>1</sup>, and Peter Reimann<sup>1</sup>  
<sup>1</sup>*Bielefeld University, Faculty of Physics, 33615 Bielefeld, Germany*  
<sup>2</sup>*Nordita, Royal Institute of Technology and Stockholm University, Roslagstullsbacken 23, SE-106 91 Stockholm, Sweden*

We conceived a model experiment for a continuous separation strategy of chiral molecules (enantiomers) without the need of any chiral selector structure or derivatization agents: Micro-particles that only differ by their chirality are shown to migrate along different directions when driven by a steady fluid flow through a square lattice of cylindrical posts. In accordance with our numerical predictions, the transport directions of the enantiomers depend very sensitively on the orientation of the lattice relatively to the fluid flow.

PACS numbers: 05.10.Gg, 05.40.Jc, 05.60.Cd

Many building blocks of life (e.g. a ligand) are organic molecules of one specific chirality which interact very differently with other molecule species (e.g. a receptor) due to their handedness (enantiomers): While one species may act as a drug, its chiral partner may be inert or even toxic [1]. Methods for separating enantiomers are thus of great importance in fields ranging from molecular biology and organic chemistry to pharmacy and agriculture. Up to date, all those methods require suitable chiral derivatization agents or some other kind of chiral selector material or structure [2]. Their main disadvantage is that they have to be developed and precisely redesigned anew for every given chiral analyte.

Here, we put forward an alternative approach which does not require any such selector with a built in *structural* chirality, but instead exploits a *dynamical* chiral symmetry breaking. The proposed model experiment from Fig. 1 builds on previous separation strategies for *non-chiral* particles, as conceived theoretically e.g. in Refs. [3, 4] and realized experimentally e.g. by Austin, Sturm, and coworkers [5]. Conceptually, our approach may be traced back to de Gennes, pointing out that small (but still macroscopic) objects of opposite chirality generically must exhibit different transport directions when sliding (or rolling) down a solid plane or floating on a liquid surface under the action of a constant force [6]. More specifically, chiral particles which are propelled in a shear flow have been explored in several theoretical [7] and experimental [8–11] studies, demonstrating that the right- and left-handed particles experience a lift force of opposite sign in the vorticity direction of the flow. For particles of one specific chirality, the resulting deflection from the main flow direction and its dependence on the shear rate was reported by Markino et al. for millimeter-sized chiral objects [10], and by Marcos et al. for micrometer-sized helical bacteria [11]. A genuine separation of right- and left-handed, centimeter-sized crystals was demonstrated by Howard [8]. Another main theoretical concept established by Kostur et al. exploits the interplay of thermal noise and of a flow field with spatially variable vorticity to separate stylized chi-

ral “molecules” [12]. In a next step, Eichhorn theoretically predicted that right- and left-handed particles are pumped with different velocities through a microfluidic channel with asymmetric walls [13].

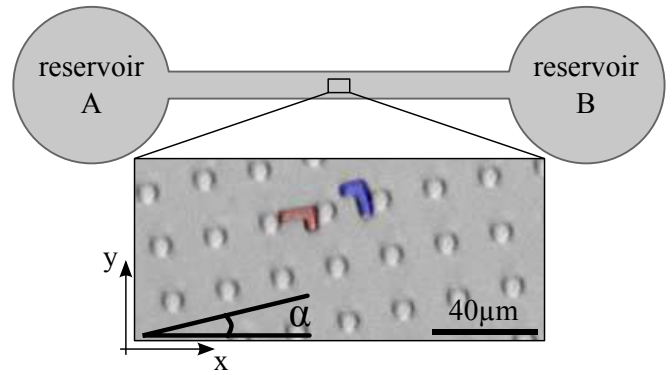


FIG. 1: Schematic top-view ( $x$ - $y$ -plane) of the microfluidic experiment with fluid- and particle-reservoirs at its ends. The magnified inset shows an optical micrograph image of the central, microstructured area (square lattice of cylindrical post) and two particles of opposite chirality. A steady fluid flow in  $x$ -direction is generated by a pneumatic pump (not shown), maintaining a constant pressure difference between the reservoirs. The angle  $\alpha$  denotes the inclination of the square lattice relatively to the fluid flow.

With our present work we further pursue yet another theoretical proposal [14], namely to employ periodic potentials for separating chiral particles. Our experimental realization of this concept is schematically illustrated in Fig. 1, featuring a central microstructured square lattice array extending over 1 cm in  $x$ -direction and 1 mm in  $y$ -direction, which consists of cylindrical posts with  $3.3 \pm 0.2 \mu\text{m}$  radius,  $20.5 \pm 0.2 \mu\text{m}$  lattice constant, and  $6 \pm 0.2 \mu\text{m}$  height ( $z$ -direction). The entire device is filled with distilled water, containing L- and  $\Gamma$ -shaped “enantiomers” in sufficiently high dilution so that their interaction can be safely neglected. Their long and short axes are  $14.7 \pm 0.3 \mu\text{m}$  and  $10.2 \pm 0.3 \mu\text{m}$  respectively, and their height ( $z$ -direction) is  $3.5 \pm 0.3 \mu\text{m}$ . Hence, they are small

enough to edge their way through the lattice and large enough to prevent their swapping of chirality by rotation about their long axis. For a more detailed description of the particle and microstructure fabrication we refer to [15]. The experiment is actuated by a pneumatic pump, maintaining a constant pressure difference of  $p \simeq 15$  mbar between the reservoirs (see Fig. 1), resulting in a steady fluid flow of the order of  $100 \mu\text{m/s}$ . During the experiment, a small part of the structured area is observed with an inverted microscope (Zeiss Axiovert 200) and the particles are tracked by digital video microscopy.

As emphasized in [14], there does not exist any symmetry argument of why the L- and  $\Gamma$ -shaped enantiomers should travel with identical mean velocities  $\bar{v}$  through the square lattice when driven by a steady flow. Following de Gennes [6], we thus can conclude that the two velocities will indeed be different unless we can name any *a priori* reasons to the contrary. One important such reason identified in [14] are locking phenomena in the absence of thermal fluctuations [4]. Since thermal noise effects turn out to be rather weak in our present experiment, the velocities of the two enantiomers are expected to be strictly speaking different but still practically indistinguishable under many conditions. To avoid such unwanted cases and rather optimize the experimental set-up *a priori*, we performed extensive numerical simulations [16]. In particular, we numerically explored many different (but still experimentally feasible) post diameters, lattice constants, particle dimensions, pressure differences, and inclination angles  $\alpha$ . In the following, we immediately focus on the resulting “best case prediction”, from which we derived the set-up specified in Fig. 1 and in the previous paragraph.

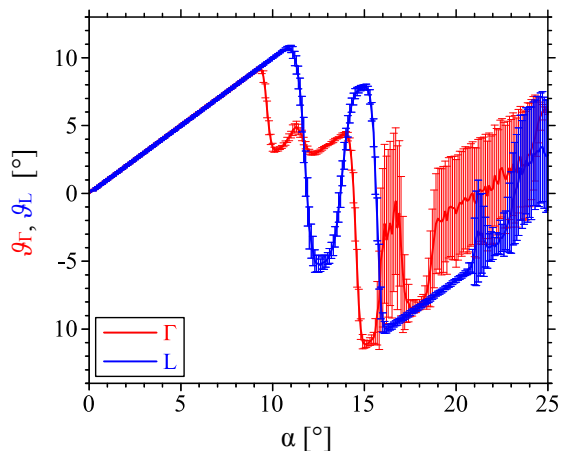


FIG. 2: Deflection angles  $\vartheta_{\Gamma}$  and  $\vartheta_{\text{L}}$  of the  $\Gamma$ - and L-shaped particles versus lattice inclination  $\alpha$ , predicted by means of numerical simulations for parameters corresponding to the experimental set-up from Fig. 1. The error bars arise by averaging over many initial conditions and realizations of the noise in combination with a long but finite temporal average.

The quantity of foremost interest is the time-averaged particle velocity  $\bar{v}$ , and in particular the deflection angle  $\vartheta$  of this velocity from the  $x$ -axis. Those numerically predicted deflection angles for both the L- and  $\Gamma$ -shaped particles versus the inclination angle  $\alpha$  of the lattice are presented in Fig. 2. For  $\alpha < 9^\circ$ , one of the above mentioned locking effects occurs: Both particle species essentially follow the (1,0) lattice direction ( $\vartheta_{\text{L}} = \vartheta_{\Gamma} = \alpha$ ), apart from extremely small deviations (not resolvable in Fig. 2) due to thermal noise. In contrast, for  $\alpha > 9^\circ$  quite appreciable differences  $\vartheta_{\text{L}} - \vartheta_{\Gamma}$  between the two transport directions arise. Beyond  $\alpha = 16^\circ$ , the error bars of  $\vartheta_{\Gamma}$  and beyond  $\alpha = 21^\circ$  also those of  $\vartheta_{\text{L}}$  dramatically increase in our simulations. The reason is that, depending on the initial conditions, numerical solutions with different time-averaged velocities  $\bar{v}$  may coexist in the absence of thermal noise. Since thermal noise is rather weak in our system, the velocities still exhibit a large variance within our quite long but still finite simulation times. To avoid such an undesirably slow convergence, we confine ourselves to  $\alpha \leq 16^\circ$ . For symmetry reasons it is furthermore sufficient to consider  $\alpha \geq 0$ .

According to Fig. 2, the largest splitting angles  $|\vartheta_{\text{L}} - \vartheta_{\Gamma}|$  between the L- and  $\Gamma$ -shaped particles are expected around  $\alpha = 15^\circ$ . A slightly weaker splitting, but remarkably enough with an opposite sign of  $\vartheta_{\text{L}} - \vartheta_{\Gamma}$ , is expected around  $\alpha = 12.5^\circ$ . Therefore, we will focus in the experiments on these two most promising values  $\alpha = 15^\circ$  and  $\alpha = 12.5^\circ$  predicted by the theory [17].

As already mentioned, we performed similar simulations as in Fig. 2 for many other lattice and particle parameters. In order to maximise  $|\vartheta_{\text{L}} - \vartheta_{\Gamma}|$ , the parameters from Fig. 2 seem to be (practically) optimal, but significant  $|\vartheta_{\text{L}} - \vartheta_{\Gamma}|$  could still be obtained for a wide range of substantially different parameters.

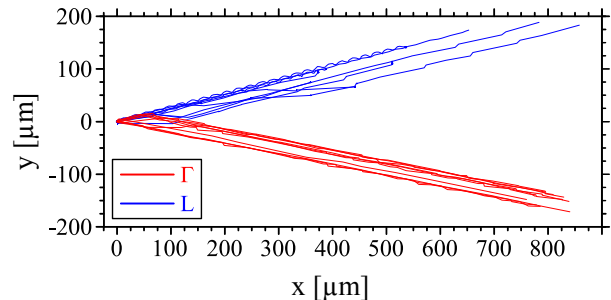


FIG. 3: Experimentally observed trajectories of L- and  $\Gamma$ -shaped particles for the same set-up as in Fig. 1 with  $\alpha = 15^\circ$ . The total length of each trajectory depends on where the particle happened to enter and exit the visual field of the optical microscope.

Fig. 3 illustrates how the L- and  $\Gamma$ -shaped particles actually move in the experiment for  $\alpha = 15^\circ$ . The main point of Fig. 3 is also the main point of our present paper: *In accordance with our numerical predictions, the*

two chiral particle species can indeed be separated from each other in our experimental microfluidic device with extremely high reliability. In fact, not a single particle with a “wrong” sign of  $\vartheta$  was observed.

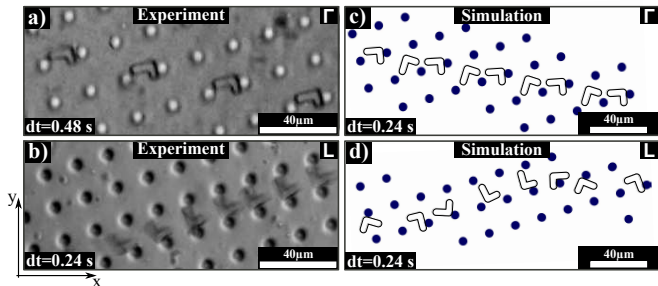


FIG. 4: Left: Stroboscopic images by superimposing several video microscopy snapshots for one  $\Gamma$ - or one L-shaped particle from Fig. 3 ( $\alpha = 15^\circ$ ). The motion proceeds from left to right at time steps  $dt$ . Right: Corresponding numerical simulations.

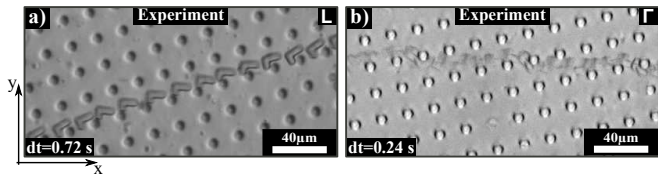


FIG. 5: (a): Same as in Fig. 4b ( $\alpha = 15^\circ$ ), but for a different video sequence of an L-shaped particle and a different time step  $dt = 0.72$  s. (b): Same as in Fig. 6a ( $\alpha = 12.5^\circ$ ), but for a different video sequence of a  $\Gamma$ -shaped particle (the snapshots are blurred due to the rapid particle motion).

Fig. 4 provides a more detailed picture of how the particles travel through the square lattice. The stroboscopic snapshots at time steps  $dt = 0.48$  s in Fig. 4a demonstrate a very regular, time-periodic motion of the  $\Gamma$ -shaped particles in the experiment. This behavior is extremely well reproduced by the simulations in Fig. 4c. The reduced time step of  $dt = 0.24$  s in Fig. 4c in addition reveals a quite pronounced rotational see-saw motion (the corresponding experimental snapshots are even more blurred than in Fig. 5b and are therefore not shown). Due to thermal noise and imperfect spatial periodicity, also very rare deviations from the behavior in Fig. 4a are observed (see also red trajectories in Fig. 3), resulting in a mean experimental deflection angle of  $\vartheta_\Gamma = -10.7^\circ \pm 0.8^\circ$ .

Turning to the L-shaped particles, Fig. 4b evidences an extremely “straight” motion along one and the same inclined row of posts. The simulation in Fig. 4d also shows short episodes of such a straight motion, but additionally every now and then the particle bumps with its “short leg” against a post, turns around, collides with another post, and finally continues along the next lower row of posts with another short episode of straight motion. In fact, the complete experimental video, of which only a small part is covered by Fig. 4b, also exhibits

such transitions between rows of posts (see also the blue trajectories in Fig. 3), but at a substantial smaller rate than in the simulations. In addition, for some of the L-shaped particles we also observed a different type of motion in the experiment, illustrated by Fig. 5a, without a comparable theoretical counterpart. (While the particles in Figs. 4b and 5a move into identical directions, their speeds (note the different time-steps  $dt$ ) and orientations differ.) Quantitatively, we thus obtained an experimental deflection angle of  $\vartheta_L = 12.1^\circ \pm 3.4^\circ$ .

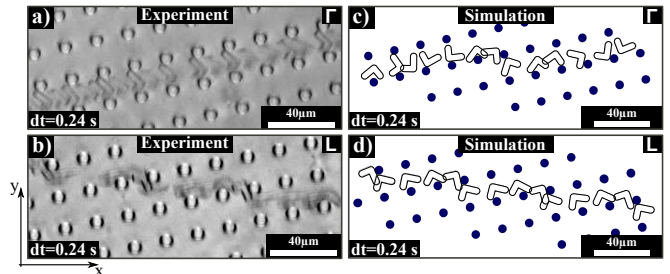


FIG. 6: Left: Same as in Fig. 4, but for  $\alpha = 12.5^\circ$ .

Similarly, Fig. 6 illustrates the experimentally and numerically observed particle motion for the second of the above predicted “most promising” deflection angles, namely  $\alpha = 12.5^\circ$ . In contrast to  $\alpha = 15^\circ$ , now the agreement between experiment and theory is excellent for the L-shaped particles, but somewhat worse for the  $\Gamma$ -shaped particles. Moreover, for the  $\Gamma$ -shaped particles there is again a second type of motion in the experiment without a theoretical counterpart, see Fig. 5b. Alternatively, the motion of the  $\Gamma$ -shaped particles predicted by the theory may be viewed as a compromise between the two experimentally observed types of motion.

We emphasize once again that the main purpose of our numerical simulations was to forecast a promising layout for our subsequent experimental realization of a microfluidic chiral selector device. In view of Fig. 3, our theoretical approach was clearly very successful in this respect. Accordingly, a further improvement of the simulated model [16] is beyond the scope of our present work. Yet, since the quantitative agreement between simulations and experiments in Figs. 2-6 is clearly not fully perfect, it is worthwhile to point out some plausible reasons. First of all, it is obvious, both from the simulations and the experiments, that quite small changes of  $\alpha$  may lead to quite notable changes of the particle velocity with respect to direction, modulus, and the co-existence (or not) of more than one “type of motion”. Numerically, a comparably sensitive dependence of the particle velocities was also observed for most of the other model parameters. One therefore expects that even quite small imperfections of the theoretical model may easily result in very significant errors of the predicted particle motion. Indeed, our model [16] involves several approximations of this kind, most notably: (i) Along the  $z$ -direction, the microfluidic device from Fig. 1 is bounded

by a “bottom-” and a “top-plane”, both of which are, however, not perfectly planar but rather exhibit notable imperfections/roughness/defects. Every now and then, a traveling particle “bumps” into one of them (due to thermal diffusion in  $z$ -direction etc.) with the result of a quite notable, sudden “deflection” (even visible under the microscope). (ii) The experimental post array deviates from a perfect square lattice and the single posts are not at all of perfect cylindrical shape. (iii) While the force exerted by the fluid flow on the particles is estimated in the theoretical model by means of the fluid flow in the absence of the particles, in reality there will be quite notable corrections due to hydrodynamic interactions between particles and microstructure. In principle, it is not difficult to account for all those effects (i)-(iii) in a theoretical model dynamics, but its numerical simulation would require (among others) to solve the full, three-dimensional hydrodynamics at every time step, which goes far beyond of what is feasible in practice. On the other hand, the qualitative and quantitative agreement between theory and experiment in Figs. 2-6 is still remarkably good in view of all those approximations (i)-(iii).

*Conclusion:* The main point of our paper was an experimental proof-of-principle that chiral particles can be separated without employing any kind of chiral selector structure but rather by exploiting a dynamical chiral symmetry breaking. In order to predict a suitable design of the experimental set-up, a simple theoretical model dynamics has been introduced and numerically solved.

Any further improvement of the various approximations of this model itself are beyond the scope of our present work. As illustrated by Fig. 3, not a single particle in the experiment exhibited a deflection angle with a “wrong” sign, i.e. the chiral separation fidelity was extremely high. A more systematic exploration and optimization of the proposed microfluidic device, e.g., with respect to some specific technological applications or a quantitative comparison with other methodologies will certainly be an important issue in the future, but goes beyond the objectives of our present study.

Besides the chiral separation *per se*, one of our main findings was that the motion of the chiral particles through the periodic microstructure depends very sensitively on the specific values of many dynamical and structural system parameters. On the one hand, the particle motion is thus very difficult to predict qualitatively by means of simple intuitive arguments and with high quantitative accuracy by means of numerical simulations. On the other hand, this sensitivity underlines the practical efficiency and variability of the experimental concept. The most promising future direction is now to downscale the generic principles behind our present approach into the realm of chiral nano-particles and molecules.

---

This work was supported by the German Research Foundation (DFG) within the Collaborative Research Center SFB 613.

- 
- [1] M. Eichelbaum, B. Testa, and A. Somogyi, *Stereochemical aspects of drug action and disposition* (Springer, 2003); E. J. Ariens, *Eur. J. Clin. Pharmacol.* **26**, 663 (1984).
  - [2] S. Ahuja, *Chiral Separation Methods for Pharmaceutical and Biotechnological Products* (John Wiley and Sons, Hoboken, 2011); G. Gübitz and M. Schmid, *Biopharm. Drug Dispos.* **22**, 291 (2001); G. K. E. Scriba, *J. Pharm. Biomed. Anal.* **27**, 373 (2002).
  - [3] D. Ertas, *Phys. Rev. Lett.* **80**, 1548 (1998); T. A. J. Duke and R. H. Austin, *ibid.* **80**, 1552 (1998); I. Derényi and R. D. Astumian, *Phys. Rev. E* **58**, 7781 (1998).
  - [4] C. Reichhardt and F. Nori, *Phys. Rev. Lett.* **82**, 414 (1999); A. M. Lacasta et al., *ibid.* **94**, 160601 (2005).
  - [5] L. R. Huang et al., *Phys. Rev. Lett.* **89**, 178301 (2002); *Science* **304**, 987 (2004); J. A. Davis et al., *PNAS* **103**, 14779 (2006); K. J. Morton et al., *PNAS* **105**, 7434 (2008); K. Loutharback et al., *Phys. Rev. Lett.* **102**, 045301 (2009).
  - [6] P. G. de Gennes, *Europhys. Lett.* **46**, 827 (1999).
  - [7] Y.-J. Kim and W. J. Rae, *Int. J. Multiphase Flow* **17**, 717 (1991); M. Doi and M. Makino, *Prog. Polym. Sci.* **30**, 876 (2005); M. Makino and M. Doi, *Phys. Fluids* **17**, 103605 (2005); N. Watari and R. G. Larson, *Phys. Rev. Lett.* **102**, 246001 (2009); C. I. Mendoza, C. M. Marques, and F. Thalmann, *Phys. Rev. E* **82**, 060401(R) (2010).
  - [8] D. W. Howard, *AIChE J.* **22**, 794 (1976).
  - [9] P. Chen and C. Chao, *Phys. Fluids* **19**, 017108 (2007).
  - [10] M. Makino, L. Arai, and M. Doi, *J. Phys. Soc. Jpn.* **77**, 064404 (2008).
  - [11] Marcos, H. C. Fu, T. R. Powers, and R. Stocker, *Phys. Rev. Lett.* **102**, 158103 (2009).
  - [12] M. Kostur, M. Schindler, P. Talkner, and P. Hänggi, *Phys. Rev. Lett.* **96**, 014502 (2006)
  - [13] R. Eichhorn, *Phys. Rev. Lett.* **105**, 034502 (2010); *Chem. Phys.* **375**, 568 (2010).
  - [14] D. Speer, R. Eichhorn and P. Reimann, *Phys. Rev. Lett.* **105**, 090602 (2010).
  - [15] L. Bogunovic et al., *J. Microelectromech. Syst.* **21**, 027003 (2011); T. Duong et al., *Microelectron. Eng.* **67-68L**, 905 (2003); A. Ros et al., *Electrophoresis* **27**, 2651 (2006); W. Hellmich et al., *J. Chromatogr. A* **1130**, 195 (2006); J. Regtmeier et al., *Euro. Phys. J. E* **22**, 335 (2007).
  - [16] The translational and rotational particle dynamics are modeled by Langevin equations [12–14], the fluid flow through the micro-lattice is determined from Navier-Stokes’ equation, and the viscous friction between fluid and particle is approximated according to the so-called shell model [18]. For more details see EPAPS Document No. [...] or [www.physik.uni-bielefeld.de/~reimann/suppl.pdf](http://www.physik.uni-bielefeld.de/~reimann/suppl.pdf)
  - [17] Note that for every  $\alpha$ -value in Fig. 1 one has to fabricate a new microstructure.
  - [18] B. Carrasco and J. G. de la Torre, *Biophys. J.* **75**, 3044 (1999).